Available online at www.sciencedirect.com
ScienceDirect
C. R. Physique 9 (2008) 788–803
COMPTES RENDUS PHYSIQUE
http://france.elsevier.com/direct/COMREN/

Recent advances in quantum dot physics / Nouveaux développements dans la physique des boîtes quantiques

Formation and ordering of epitaxial quantum dots

Paola Atkinson [a,*], Oliver G. Schmidt [b], Stephen P. Bremner [c], David A. Ritchie [c]

[a] *Max Planck Institute for Solid State Research, Heisenbergstrasse 1, 70563 Stuttgart, Germany*
[b] *Institute for Integrative Nanosciences, IFW Dresden, Helmholtzstr. 20, 01069 Dresden, Germany*
[c] *University of Cambridge, Cavendish Laboratory, JJ Thomson Avenue, Cambridge, CB3 0HE, UK*

Available online 21 November 2008

Abstract

Single quantum dots (QDs) have great potential as building blocks for quantum information processing devices. However, one of the major difficulties in the fabrication of such devices is the placement of a single dot at a pre-determined position in the device structure, for example, in the centre of a photonic cavity. In this article we review some recent investigations in the site-controlled growth of InAs QDs on GaAs by molecular beam epitaxy. The method we use is ex-situ patterning of the GaAs substrate by electron beam lithography and conventional wet or dry etching techniques to form shallow pits in the surface which then determine the nucleation site of an InAs dot. This method is easily scalable and can be incorporated with marker structures to enable simple post-growth lithographic alignment of devices to each site-controlled dot. We demonstrate good site-control for arrays with up to 10 micron spacing between patterned sites, with no dots nucleating between the sites. We discuss the mechanism and the effect of pattern size, InAs deposition amount and growth conditions on this site-control method. Finally we discuss the photoluminescence from these dots and highlight the remaining challenges for this technique. ***To cite this article: P. Atkinson et al., C. R. Physique 9 (2008).***

Résumé

Croissance et contrôle des boîtes quantiques épitaxiales. Les boîtes quantiques uniques présentent un grand intérêt potentiel comme brique de base des composants pour l'information quantique. Cependant, une des difficultés majeures dans la réalisation de ces composants, est le positionnement de la boîte à un endroit prédéterminé dans la structure du composant, par exemple au centre d'une cavité photonique. Dans cet article, nous présentons quelques travaux récents pour le contrôle de la croissance de boîtes InAs/GaAs sur des sites prédéterminés, lors de l'épitaxie par jets moléculaires. La méthode utilisée est la gravure ex-situ d'un substrat de GaAs par lithographie électronique, suivie de techniques de gravure sèche ou humide pour former des petits trous à la surface de GaAs, qui agissent comme site de nucléation pour les boîtes d'InAs. Cette méthode est facilement ajustable et peut être appliquée avec des structures-repère permettant un alignement lithographique après croissance des composants avec chaque site prédéterminé de boîte. Nous montrons qu'un bon contrôle des sites de croissance (sans nucléation de boîte entre les sites) est possible pour des matrices présentant un espacement entre sites jusqu'à 10 microns. Nous discutons du mécanisme de la croissance contrôlée sur site en fonction de la taille du motif, de la quantité d'indium déposée, et des conditions de croissance. ***Pour citer cet article : P. Atkinson et al., C. R. Physique 9 (2008).***

* Corresponding author.
E-mail address: P.Atkinson@fkf.mpg.de (P. Atkinson).

1631-0705/$ – see front matter
doi:10.1016/j.crhy.2008.10.014

Keywords: Quantum dot; Molecular beam epitaxy

Mots-clés : Boîte quantique ; Épitaxie par jets moléculaires

1. Introduction

Self-assembled quantum dots (QDs) such as InAs/GaAs QDs have been the subject of intensive research for several years. Part of this research has been focused on studies of single quantum dots, increasingly motivated by the possibility of using these QDs as single photon sources for quantum information processing [1–3]. This has, in turn, led to increasing interest in controlling the position of semiconductor quantum dots [4] so that they can be incorporated deterministically into devices. Precise control over the location of a single dot is particularly important for photonic cavity device structures, since the enhancement of spontaneous emission provided by the photonic cavity mode depends critically on the dot location [5].

Techniques exist to accurately locate a buried QD *post-growth* with respect to marker structures, using either the position of the dot luminescence [6] or of a small surface mound above the dot [7]. This has enabled the successful alignment of a photonic crystal over a dot, and strong coupling of the dot to the cavity has been demonstrated [7]. However, not only is this process very time-intensive, it is also not easily scalable. It would be preferable instead to position the quantum dots themselves at pre-determined locations with respect to marker structures. It would then be a relatively simple matter to align an array of cavities over an array of such site-controlled dots. The growth of site-controlled InAs/GaAs dots for this purpose is the main subject of this paper and is compared with the growth of conventional, randomly positioned, dots.

2. Stranski–Krastanov growth of InAs quantum dots

The growth of InAs QDs on GaAs has been described in great detail elsewhere (see for example Refs. [8–10]), so we will only briefly mention some of the main features of quantum dot growth here for comparison later with observations of site-controlled dot growth.

InAs initially grows in a layer-by-layer fashion on GaAs until some critical thickness of InAs has been deposited at which point 3D islands form as shown schematically in Fig. 1(a). The critical thickness, (C_{crit}) typically 1.5–1.7 ML, is independent of temperature, although the amount of InAs that must be supplied increases with temperature due

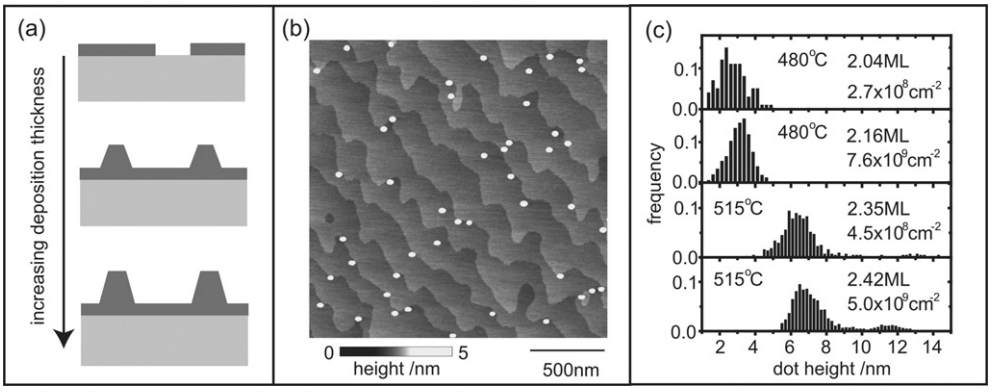

Fig. 1. (a) Schematic of the Stranski–Krastanov growth mode of dot formation, showing initial layer by layer growth followed by 3D island formation and growth with the presence of a 2D wetting layer between the islands. (b) AFM image of randomly positioned InAs dots grown on GaAs. Almost all these dots have nucleated by a step edge. (c) Histograms showing the height distribution of InAs quantum dots at different growth temperatures and amount of InAs supplied. The InAs growth rate was ∼0.01 ML/s. The density increases rapidly with small increases in InAs deposition, whereas there is a much smaller increase in dot size. The amount of InAs that must be supplied to achieve the same dot density increases with temperature due to increased InAs desorption. The dot size increases with increasing growth temperature and the onset of a bimodal dot size distribution can be seen in the lower panel.

to increasing Indium desorption [11]. This behaviour is known as Stranski–Krastanov growth and is a strain-driven process, due to the 7% lattice mismatch between InAs and GaAs.

Once dot nucleation occurs, the dots form near-randomly over a flat surface with some preference for nucleation at step edges [12–14], as shown in Fig. 1(b), due to the energy barrier for downward hopping at step edges which leads to a local accumulation of adatoms above the step. For high dot densities some ordering of the dots along the $\langle 100 \rangle$ directions has also been observed due to elastic strain interactions in the substrate [15]. Both these effects, preference of nucleation at step edges and local ordering due to strain interactions have been used to create locally ordered, dense arrays of dots by the use of both vicinal substrates and stacked layers of dots [16,17].

The dot density increases very rapidly, from zero to $> 10^{10}$ cm^{-2} for less than 0.2 ML InAs additional deposition and the increase in total dot volume is much larger than the additional amount of InAs supplied. This is due to several tenths of a monolayer of InAs floating on the growth surface which transfers from the 2D wetting layer into the dots (see for example [9,14] and references therein). Both the dot size and the dot density can be controlled by the growth conditions. Increasing the growth temperature leads to a decrease in the dot density and an increase in the dot size for a given deposition amount as demonstrated in Fig. 1(c). It can also be seen that the dot size increases much more slowly than the dot density for a range of growth conditions [12]. Decreasing the growth rate leads to an increase in dot size and a decrease in dot density as it eventually becomes more favourable for adatoms to attach to existing dots rather than nucleating new dots [18,19].

With increasing deposition amount the dots change shape from low-angle facetted pyramidal dot shapes to higher-angle facetted dome-like dot shapes [20,21]. The same dot shapes have been observed on dense arrays of site-controlled dots [22]. Depending on the growth conditions, the dot height distribution can either be multimodal [21], bimodal as shown in Fig. 1(c) [23,24] or narrow [25]. Low growth rate ($\ll 0.01$ ML/s) conditions force the distribution to consist of mainly the steeper facetted dome-like dots [19]. As the deposition amount increases further, dots begin to coalesce forming incoherent dots which then rapidly grow in size due to the presence of dislocations which act as efficient capture sites for adatoms [12]. This coalescence occurs sooner at lower growth temperatures [26].

3. Site-control of dot nucleation

Several methods of controlling the nucleation of quantum dots have been proposed and demonstrated in the literature (see e.g. [4]). These methods are based on one of three main mechanisms or a combination thereof – modification of the surface step morphology, the surface curvature, or the underlying strain of the substrate. These mechanisms control the dot nucleation site by either altering the indium adatom migration, leading to local areas of material accumulation such that the critical thickness for dot formation is exceeded in locally defined areas, or by locally changing the strain such that the critical strain for dot formation is reached earlier, i.e. for lower deposition amounts, in certain areas.

Methods demonstrated include the use of vicinal substrates (e.g. [27]), strain modulated buffer layers (e.g. [17, 28,29]), the etching of mesas or trenches (e.g. [30,31]) and the patterning of small holes by focused ion beam [32], scanning probe techniques [33,34], or electron-beam lithography [33,35–40].

Long range perfect ordering has been demonstrated for dense (~ 200 nm spacing) arrays of quantum dots [36,37] using electron-beam patterned substrates to define the positions of the dots. However the growth conditions required for this perfect ordering result in a relatively high dot density of randomly distributed dots outside the patterned area [22].

We discuss here the alternative case of growth of a dilute ordered array – with the ultimate aim of placement of single, or pairs of, InAs quantum dots such that they can be individually addressed either optically or electrically in a device structure. This puts a lower bound on the spacing of the ordered array to ~ 2 microns, together with the requirement that the unintentional, i.e. non site-controlled, dot density must be much less than the density of the site-controlled dots i.e. $\ll 2 \times 10^7$ cm^{-2}.

To achieve this we use conventional electron-beam lithography together with standard dry or wet etching techniques to pattern a GaAs substrate with small holes prior to growth. These small holes infill with In(Ga)As during initial GaAs buffer and InAs growth. These infilled pits thereby locally modify the surface strain, leading to preferential dot-nucleation over the patterned sites, prior to dot formation elsewhere.

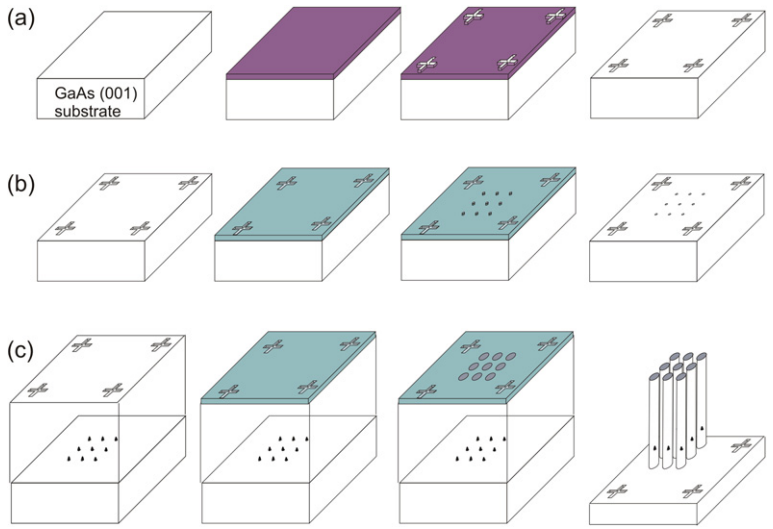

Fig. 2. Process flow schematic for placing site-controlled dots in micropillar microcavities. The first row (a) depicts a photolithography stage to define alignment markers etched deep into a buffer layer (e.g. a bottom DBR). The second row (b) depicts the e-beam lithography stage needed to define the pits for dot site control. These are positioned with respect to the alignment markers. The third row (c) depicts the post-growth processing, which consists of an e-beam lithography stage to define the pillars. These are again positioned with respect to the initial alignment markers. The alignment of pillar to site-controlled dot should agree to within the accuracy of the e-beam system, typically a few tens of nm. The color layers correspond to the photoresists.

3.1. Experimental details

3.1.1. Substrate patterning

The patterned substrates were prepared by standard electron-beam lithography and either dry or wet chemical etching. The advantage of using standard ex-situ patterning techniques is that it is a well-defined process to create, and subsequently use, alignment marks to align the site-controlled dots with further device processing post-growth. This process is illustrated in Fig. 2.

Initially, a GaAs buffer or the bottom half of a device structure, for example the bottom distributed bragg reflector (DBR) of a microcavity, is grown on a GaAs (001) substrate. Standard UV photolithography (Fig. 2(a)) followed by $SiCl_4$ reactive ion beam etching can be used to define deep (> 250 nm) alignment markers in the substrate. The substrate is then ultrasonically cleaned using a series of heated solvents (acetone at 50 °C, n-methyl-pyrollidone at 70 °C and isopropanol at 50 °C) followed by an oxygen plasma ash to remove any residual resist and a dilute hydrochloric acid dip (1HCl:3H_2O) followed by a rinse in de-ionized water to remove the oxide formed by the plasma treatment.

The sample is then covered with thin (~ 70 nm thick) polymethylmethacrylate (PMMA) resist and patterned by electron-beam lithography with an array of holes whose position is defined with respect to the pre-patterned alignment markers. The pattern is then transferred to the substrate either by $SiCl_4$ reactive ion beam etching or by wet etching using a 1:8:800 H_2SO_4:H_2O_2:H_2O solution to give pits in the surface 80–120 nm wide and ~ 20–30 nm deep. Wet chemical etching with 1:8:800 H_2SO_4:H_2O_2:H_2O solution has the advantage that the etch rate, ~ 1 nm/s, is highly controllable, however it does lead to an increase in the average hole width of ~ 20–40 nm due to lateral undercutting of the resist unlike in the case of dry-etched holes. The sidewall angle is also shallower after wet-etching, typically 20–30° to the horizontal, compared to $\sim 40°$ to the horizontal after dry-etching. The distribution of the hole widths after patterning, irrespective of the etching method used, had a full-width at half maximum of ~ 10 nm.

The substrate is then cleaned again by a series of heated solvents, an oxygen plasma ash and a dilute hydrochloric acid dip. If the resist has been fully removed from the surface then it can be seen that the surface is hydrophilic after the dilute hydrochloric acid treatment [41], and the GaAs step edges of the original buffer can be observed in AFM measurements. The substrate is then loaded into the ultra-high vacuum system ready for overgrowth. As shown in Fig. 2(c), once the epitaxial layers have been grown on the patterned substrate, the sample can be processed

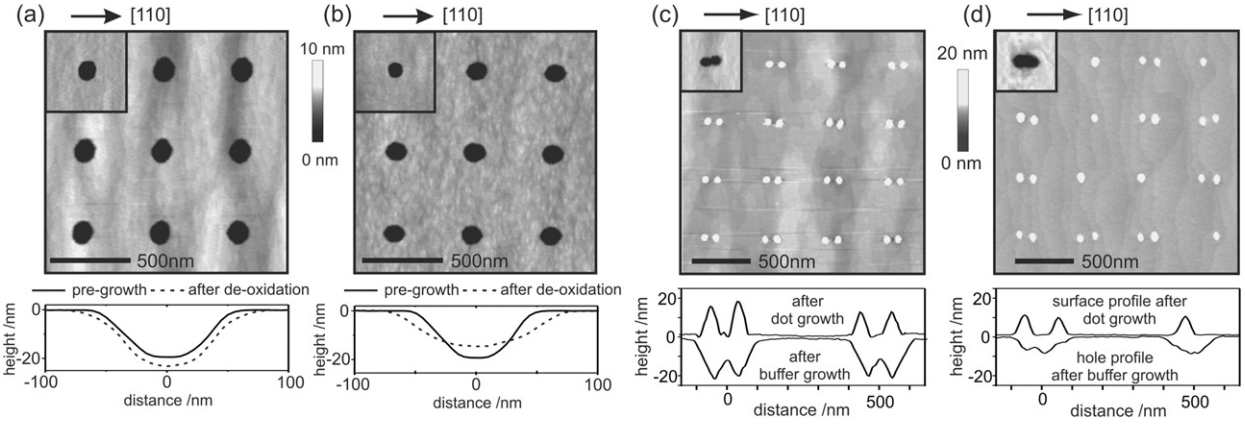

Fig. 3. AFM images and line profiles of holes ∼100 nm wide, 20 nm deep (a) after H-assisted deoxidation at ∼400 °C and a brief thermal anneal. (b) after Ga-assisted deoxidation using 6 ML Ga deposited at ∼460 °C and a brief thermal anneal. (c) after H-assisted deoxidation, 10 nm GaAs buffer growth and ∼1.4 ML InAs deposited at ∼510 °C. (d) after Ga-assisted deoxidation, 8 nm GaAs buffer growth and ∼1.4 ML InAs deposited at ∼510 °C [43]. The insets show the hole shape (a), after patterning (b), and after GaAs buffer growth (c), (d). Part reprinted from [43] with permission from Elsevier.

into devices, in this example micropillar microcavities, using the original deep-etched alignment marks to locate the position of the buried site-controlled dots.

3.1.2. Surface oxide removal

Before overgrowth can be carried out, the surface oxide needs to be removed from the patterned substrate. Conventional thermal deoxidation, which is carried out at a substrate temperature of ∼580 °C under an arsenic overpressure leads to pitting of the surface [42] due to the most stable surface oxide Ga_2O_3 reacting with the substrate to form the more volatile oxide Ga_2O i.e. $Ga_2O_3 + 2GaAs \rightarrow 3Ga_2O + As_2$. These surface pits subsequently prevent good quantum dot site-control from being achieved during overgrowth on a patterned substrate by competing with the patterned sites for capture of adatoms [43].

The surface oxide can instead be removed by exposure to a hydrogen atom flux of 10^{-4}–10^{-3} mbar at a substrate temperature of ∼400–500 °C. This reduces the stable surface oxide by the reaction $Ga_2O_3 + 4H \rightarrow Ga_2O + 2H_2O$ leading to a clean, undamaged oxide-free surface. We have used both thermally cracked hydrogen atom beams (created by passing hydrogen gas over a heated tungsten filament) and rf generated hydrogen plasma sources (where the hydrogen is dissociated by application of rf power) to successfully remove the surface oxide *in-situ*. This deoxidation technique leads to a slight increase (∼5 nm) in width and depth of the patterned holes due to removal of the oxide but otherwise leaves the pattern undamaged, as shown in Fig. 3(a) [44]. Care however must be taken to avoid surface contamination being introduced during the hydrogenation [45] and the hydrogen dose should be carefully controlled to avoid degradation of the surface occurring due to loss of arsenic [46,47].

An alternative method of oxide removal is to use gallium to reduce the stable oxide, in the absence of arsenic, by the reaction $Ga_2O_3 + 4Ga \rightarrow 3Ga_2O$ [42,48]. Typically we observe that nearly two monolayers of Ga_2O_3 forms on the surface during a ∼1 hour air exposure between the final HCl dip and loading the sample into the vacuum system. This thin oxide layer can be removed by 6–8 ML of Ga supplied at a substrate temperature of ∼420–460 °C without leading to pitting of the surface. This deoxidation method leads to a slight flattening of the hole profile with a ∼3 nm decrease in depth and an increase in width of ∼10 nm as shown in Fig. 3(b) due to some gallium accumulation at the bottom of the hole. This small change in shape does not prevent the patterned holes from being used to control the quantum dot position as shown in Fig. 3(d), as long as the GaAs buffer thickness is also reduced i.e. from ∼ 10 nm (Fig. 3(c)) to ∼8 nm (Fig. 3(d)) [43]. Gallium-assisted deoxidation has the basic advantage that it can be carried out in the growth chamber, with the oxide removal being monitored *in-situ* by reflection high energy electron diffraction (RHEED), with no need for additional apparatus (such as a hydrogen source and a turbo pump). The disadvantage however is that it is very sensitive to the amount of oxide on the surface. If more hydrogen is supplied than is required to fully reduce the surface oxide during hydrogen-assisted deoxidation then there is no additional change in hole shape. However, if excess gallium is supplied then the hole begins to infill [43].

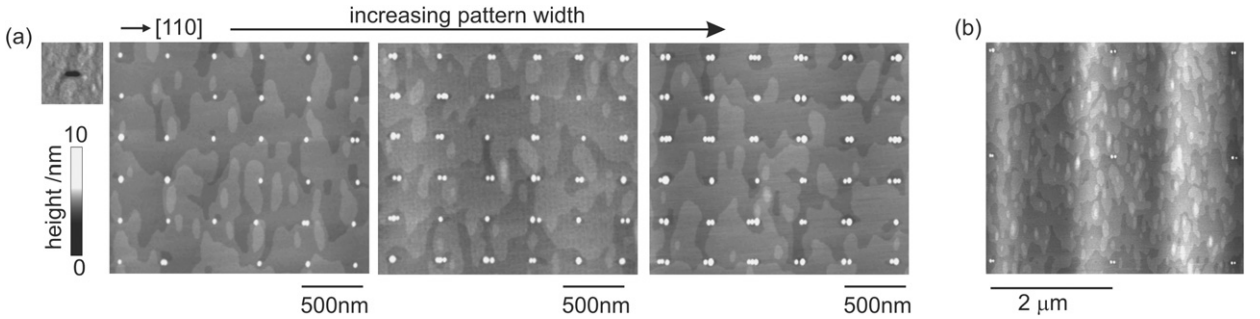

Fig. 4. AFM images of patterned samples following 10 nm GaAs buffer growth and after 87% of the critical thickness of InAs was deposited. (a) (left to right) AFM image of the shape of the hole after the buffer growth, of the dot occupancy on patterns 35 nm deep and ∼60 nm wide, ∼70 nm wide and ∼80 nm wide on a 400 nm spaced array. (b) AFM image of the dot occupancy on a 2 micron spaced array of patterns ∼70 nm wide and ∼35 nm deep.

3.1.3. GaAs buffer overgrowth

Samples were grown either in a VG V80H or Riber 32P growth chamber. After low-temperature deoxidation (either H-assisted, or Ga-assisted) the samples were briefly annealed for 2–5 minutes at ∼560 °C under an As_4 overpressure to ensure that all the oxide had been removed and/or to recrystallize any excess gallium that may have been deposited in the case of Ga-assisted deoxidation [48]. This thermal anneal leads to a slight rounding of the hole profile [44,37] due to some bulk diffusion occurring but is otherwise brief enough to prevent any significant damage to the pattern. If the anneal time is increased to 30 minutes then significant surface roughening occurs around the patterns, preventing the pattern array from controlling the InAs quantum dot site.

After this brief thermal anneal, the substrate temperature was reduced to 500–515 °C as measured either by Band Edge Thermometry or by the RHEED transition between the $c(4 \times 4)$ and (2×4) reconstructions. A thin GaAs buffer, ranging from 7 nm–12 nm thick depending on the initial depth of the hole, was then grown. The GaAs growth rate was 0.5–0.6 ML/s and the V/III flux ratio was typically ∼24.

This buffer growth is important since there are generally small pits on the surface following deoxidation, such that a buffer thickness > 6 nm is necessary to prevent unintentional dots nucleating between the patterns of a dilute array [49]. The buffer also allows the InAs dots to be situated some distance away from the regrowth interface and any defects located there which could act as non-radiative recombination centres and degrade the luminescence characteristics. These defects are likely to be Ga and As antisite defects due to some disorder in the surface which occurs during oxidation [50] and can be still observed in the reconstruction following deoxidation [51].

The effect of this buffer growth on the hole shape is shown in the insets to Figs. 3(c) and 3(d). The holes become shallower and change shape forming a "figure-of-eight" due to preferential migration of gallium adatoms away from A-type (Ga-terminated) sidewalls and towards B-type (As-terminated) sidewalls [52]. This competition between the different migration directions on the different facets means that the change in shape is affected by the hole size, with the "figure-of-eight" shape becoming more marked for wider holes (>100 nm wide) [38] and can also be affected by the growth conditions. This is due to the fact that the preferential migration towards B-type sidewalls depends on the As_4 overpressure and can be reversed at either very high or very low overpressures [52,53].

For example, we have observed that if As_2 is used there is always net migration away from both A- and B-type sidewalls. This leads to the holes increasing in size during the buffer growth, making it impossible for them to act as sites for single-dot nucleation. We have also observed that the "figure-of-eight" shape appears to be more clearly defined if As_4 from a conventional thermal arsenic source is used rather than from an arsenic cracker source for similar initial pattern sizes. This difference can be seen by comparing the shape of the hole after the buffer growth in Fig. 3(c) (thermal source) and Fig. 4(a) (cracker source). This effect may be due either to the presence of a small fraction of As_2 coming from the cracker source even when the cracker zone is run at a relatively low temperature (typically ∼500–600 °C) or, more likely, is due to the fact that the As_4 molecules coming from the cracker source are more energetic due to the additional heating at the cracker zone. The more energetic As_4 molecules will dissociate easier at the substrate to form the As_2 precursor, thus changing the local III-V ratio and the incorporation probability on As-terminated step edges [54,55].

If the hole is shallow enough ($\sim$3–6 nm deep) after the buffer growth then it infills during the InAs growth due to net migration towards the bottom of the hole driven by the lower surface energy due to the concave surface curvature [56]. This infilled area then acts as the nucleation site for dots and is the scenario which we will consider in more detail later.

If instead the hole is still quite deep ($>$15 nm) after the buffer growth, then enough InAs will accumulate at the bottom of the hole to reach the critical strain for dot formation before the hole has infilled. As long as the lateral dimensions of the hole are small enough (less than $\sim$60 nm wide), then this hole can still act as a preferential site for a single dot as can be seen by the dot formation over each half of the "figure-of-eight" shaped hole in Fig. 3(c).

If the hole is larger i.e. still $>$15 nm deep and $>$100 nm wide after the buffer growth then we typically see large incoherent dots at the bottom of the hole formed by several dots forming and coalescing due to the large amount of InAs that has accumulated there. A few dots also nucleate around the edges of the larger holes if they have not infilled due to the high step density of B-type step edges exposed there.

The change in shape of the hole during buffer growth limits the maximum thickness of the grown buffer to $\sim$20 nm, since otherwise the holes become too shallow to act as preferential nucleation sites. This cannot be adequately compensated for by increasing the initial hole depth since the net adatom migration away from A-type facets during the growth of a thicker GaAs buffer over a deeper hole results in a large increase in width in the [$-$110] direction leading to a chain of dots nucleating over each patterned site.

This limitation on the buffer thickness imposed by the change in shape of the holes is due to the use of the (100) GaAs substrate which means that different facet types (As-terminated and Ga-terminated) are present on the edges of the etched holes. Such a limitation may be avoided if a different substrate orientation is used, as demonstrated by MOVPE growth of site-controlled dots using triangular etched pits on (111)B substrates, where only (111)A facets are exposed and the hole shape is maintained during overgrowth [57].

3.1.4. InAs overgrowth

Following the GaAs buffer growth, InAs was then deposited at the same growth temperature of $\sim$500–515 °C, with a growth rate of 0.0075–0.009 ML/s unless otherwise stated in the text. During InAs growth the V/III pressure ratio was typically in the range 400–800. In general, the amount of InAs deposited was $\sim$85–95% of the critical thickness (C_{crit}) for dot formation on an unpatterned surface, such that almost no dots were observed outside the patterned areas i.e. the dot density on unpatterned regions ranged from 0–5 $\times$ 10^6 cm^{-2} for all the samples discussed.

In general, we always observe a range of dot occupancy over the patterned sites due to fluctuations in the initial pattern size. We have observed up to 60% single dot occupancy on patterns 60 nm wide, 35 nm deep and on patterns 90 nm wide, 20 nm deep using an As cracker source [39], and close to 100% double dot occupancy on wet-etched patterned holes 110 nm wide, 20 nm deep using a conventional thermal arsenic source [58] where the "figure-of-eight" shape of the holes is better defined leading to more controlled double-dot occupancy.

An example of the high degree of selectivity of dot formation is shown in Fig. 4. For the smallest pattern size in Fig. 4(a) ($\sim$60 nm wide, 35 nm deep) a large proportion of sites contain a single dot, some sites contain a pair of closely spaced dots (spacing $\sim$30 nm), some of which seem to be on the verge of coalescing, and some sites contain no dot but the hole is completely infilled with In(Ga)As. As the pattern size increases, by only $\sim$10 nm in width, it can be seen that more sites are occupied by two dots, and then by three dots which are aligned along [110] due to the hole shape which is elongated in this direction as shown in Fig. 4(a). This site-control is not dependent on the pattern spacing, as shown by Fig. 4(b) where as good site-control is demonstrated on a 2 micron spaced array as on a 500 nm spaced array. The effect of the pattern size, InAs deposition amount and the growth conditions on the dot occupancy and dot size will be discussed in more detail in the following sections.

3.2. Effect of pattern size and InAs deposition amount

Fig. 5(a) shows the range of occupancy observed for different hole widths for two different pattern depths after $0.87C_{\text{crit}}$ InAs was deposited [39]. The mode of the distribution is seen to increase by one for only a $\sim$10 nm increase in hole width, with the single dot occupancy being highly sensitive to the initial patterned hole size, dropping from $>$50% to $<$20% for differences in average hole width of only $\sim$20 nm. The occupancy is also dependent on the hole depth, with a decrease in hole depth leading to a decrease in occupancy. This dependence on hole depth means that the occupancy can also be increased by reducing the buffer thickness [49]. The sensitivity of the occupancy to such

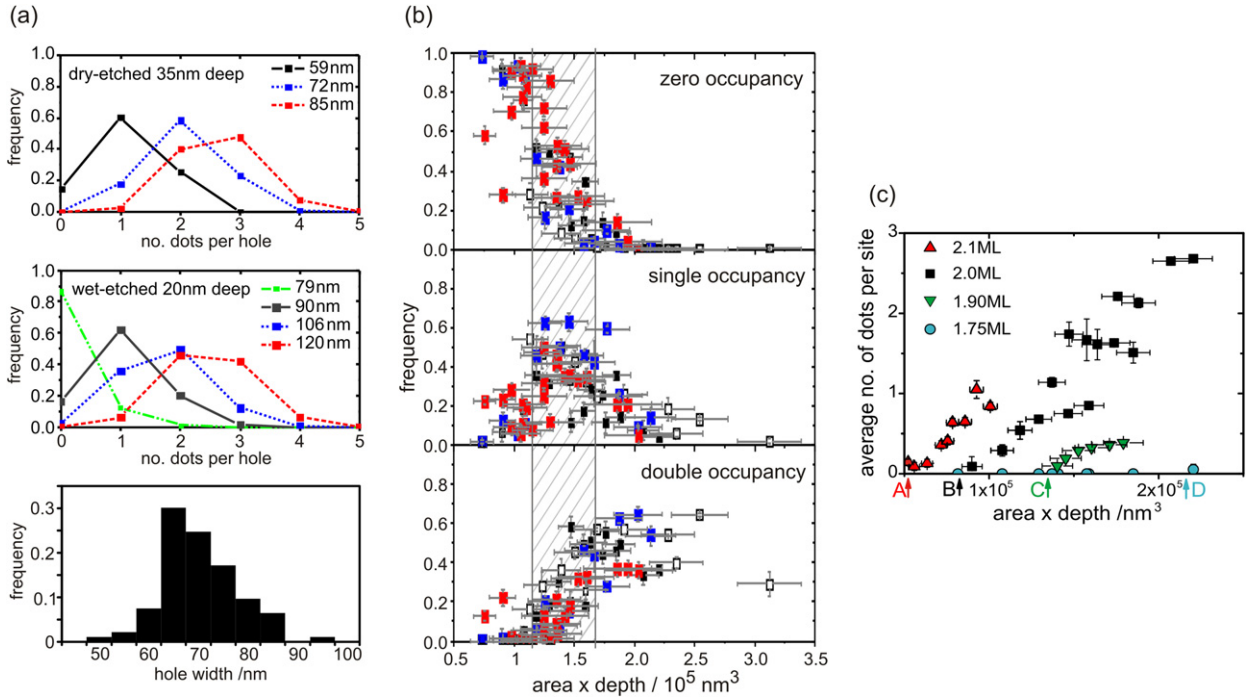

Fig. 5. (a) (Top panel and middle panel) Dot occupancy statistics for different initial hole widths for two differently patterned samples. Over 500 holes were measured for each data set [39]. (Bottom panel) Range of hole sizes for a given nominal pattern size after patterning. (b) Percentage of holes containing none, one or two dots as a function of initial hole area × depth. Different symbols correspond to different patterned samples. The shaded region denotes where the single dot occupancy is approximately 30% or greater. Reproduced with permission from [39]. (c) Graph showing the average number of dots per patterned site as a function of initial hole area × depth for different InAs coverages. Arrows marked A, B, C and D correspond to the pattern sizes at which dot formation begins to occur for 2.1, 2.0, 1.9 and 1.75 ML InAs deposition, respectively. The critical thickness under these growth conditions was 2.3 ML InAs deposition (neglecting indium desorption). Reprinted from [49] with permission from Elsevier.

small changes in hole size explains why a range in occupancy is seen, since the spread in patterned hole size is also of the order of ± 10 nm as shown in the lower panel of Fig. 5(a).

Since patterning such small holes reliably is non-trivial, it would be useful to be able to predict the occupancy of a particular pattern size from a simple pre-growth measurement of the hole sizes, so that the growth conditions could then be tuned accordingly. The preferential dot nucleation above these patterned sites is believed to be driven by the strain difference above an infilled hole compared to the surrounding planar region. If we assume that the magnitude of this strain difference is related to the depth of the hole and consider that the net amount of InAs which will accumulate over each infilled hole must be related to the area over which this driving force is acting, then it seems reasonable to expect that the product of the depth of the hole and its area can be used to determine the probability of nucleating one or more dots at each site.

Fig. 5(b) shows a plot of dot occupancy vs. hole area × depth for seven patterned wafers, all with depths ranging between 15–35 nm deep. The dotted lines and dashed area demarcate a range of hole sizes where >30% single dot occupancy would be expected to be observed for 0.87 C_{crit} InAs deposition which would already provide a significant improvement in the processing yield of single-dot devices [39].

Although this is mostly a qualitative description since no account is taken of the change in hole shape during deoxidation and buffer growth and the measurements used are of the initial depth of the hole and the initial area as projected on (100), there is good agreement between differently patterned wafers. This allows us to gain some predictive insight into the dot distribution expected post-growth from simple pre-growth measurements and also means that we can use the product of the area and depth of the holes prior to growth to compare samples with slightly different pattern dimensions.

Fig. 5(c) shows the average dot occupancy of a patterned site for a range of hole sizes for four different deposition amounts. The occupancy can be increased either by increasing the pattern size for a given InAs coverage as shown

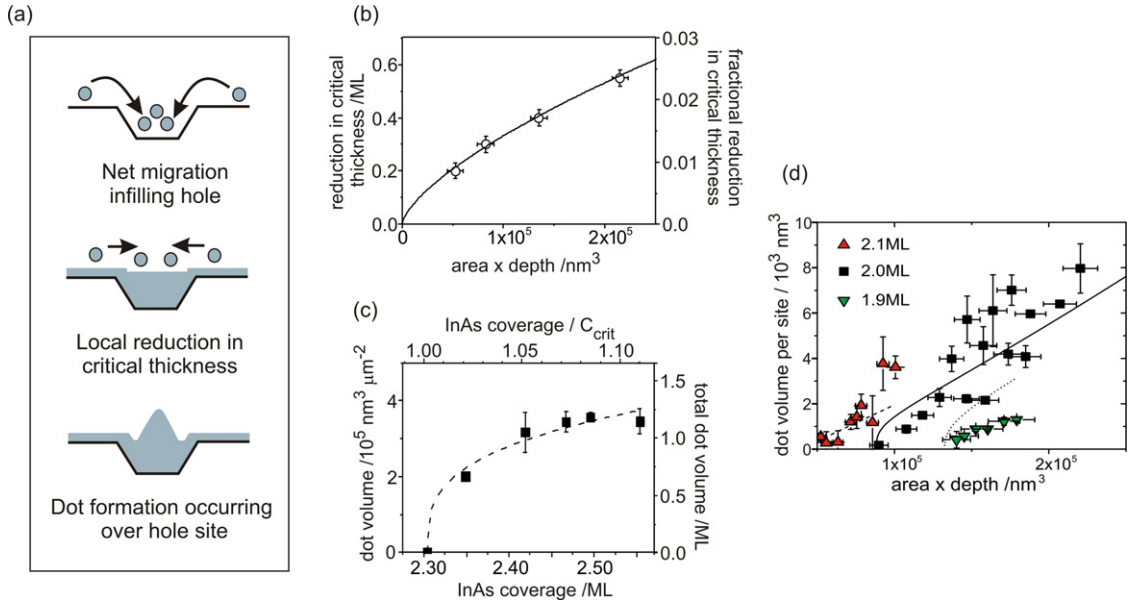

Fig. 6. (a) Schematic diagram of the mechanism for site-controlled InAs dot formation. (b) Graph showing reduction in critical thickness for dot formation for different values of initial hole area × depth. The best-fit line shown is a power-law fit of the form: $\Delta C_{\text{crit}} = \alpha S^{\beta}$ [49]. (c) Graph showing average InAs dot volume per unit area as a function of InAs coverage on an unpatterned surface. Incoherent dots were observed to form at coverages >2.5 ML. The best-fit line shown is of the form: $V = A(C - C_{\text{crit}})^{p}$ [49]. (d) Graph of average dot volume per patterned site vs. initial hole area × depth for different InAs coverages. The curves correspond to the model function $V = sA(C - [C_{\text{crit}} - \alpha S^{\beta}])^{p}C$, the InAs coverage, is set as 1.9 ML (dotted line), 2.0 ML (solid line) and 2.1 ML (dashed line). The parameters for all the best fit lines are given in the text. Part reprinted from [49] with permission from Elsevier.

already, or conversely by increasing the coverage for the same pattern size [49]. This means that for a range of pattern sizes the deposition amount can be tuned to give good site-control of quantum dots.

3.3. Mechanism of site-control

Patterned sites which contain no dots show that the holes are completely infilled during the InAs deposition. These infilled holes subsequently act as preferential nucleation sites for dot formation due to the difference in strain above the infilled hole and the surrounding planar area as shown schematically in Fig. 6(a). This has also been observed on holes 4 nm deep, 27 × 42 nm wide patterned by a scanning probe technique, where evidence of strain in the infilled site could be resolved by *in-situ* scanning tunneling measurements as a slight (< 1 ML) outward bulging of the surface [33]. If we imagine that the strain due to the In(Ga)As in the infilled hole reduces the amount of InAs that subsequently needs to be deposited over the patterned site before dot formation occurs then we can define a local reduction in critical thickness due to the infilled site.

By looking at the data shown in Fig. 5(c) the critical pattern size for dot formation (labeled A, B, C and D) can be obtained for different InAs coverages, allowing a reduction in critical thickness as a function of pattern size to be quantified as shown in Fig. 6(b). We fit this data using a power-law fit of the form $\Delta C_{\text{crit}} = \alpha S^{\beta}$ where $\alpha = (1.3 \pm 0.5) \times 10^{-4}$ ML/nm^3 and $\beta = (0.68 \pm 0.04)$ [49]. ΔC_{crit} is the reduction in the critical thickness and S is the hole size. We also consider the growth of quantum dots on an unpatterned region under the same growth conditions, shown in Fig. 6(c), which is approximately fitted by a power-law of the form $V = A(C - C_{\text{crit}})^{p}$ [12] where $A = (6 \pm 8) \times 10^5$ nm^3/µm^2 and $p = (0.31 \pm 0.08)$, V is the average dot volume per unit area, C is the InAs coverage and the critical thickness $C_{\text{crit}} = 2.3$ ML (neglecting the effect of indium desorption).

If, apart from a local reduction in critical thickness over the infilled pattern site, the site-controlled dots grow as on an unpatterned region then we can simply model the dependence of dot volume on pattern size and deposition amount as $V = sA(C - [C_{\text{crit}} - \alpha S^{\beta}])^{p}$ [49]. V is the average dot volume per patterned site in this case, s is the patterned site area and all the other parameters are as previously defined. It can be seen from Fig. 6(c) that there is good agreement between this simple model and the experimental data for the 2.0 ML ($0.85C_{\text{crit}}$) data given the errors in the parameters

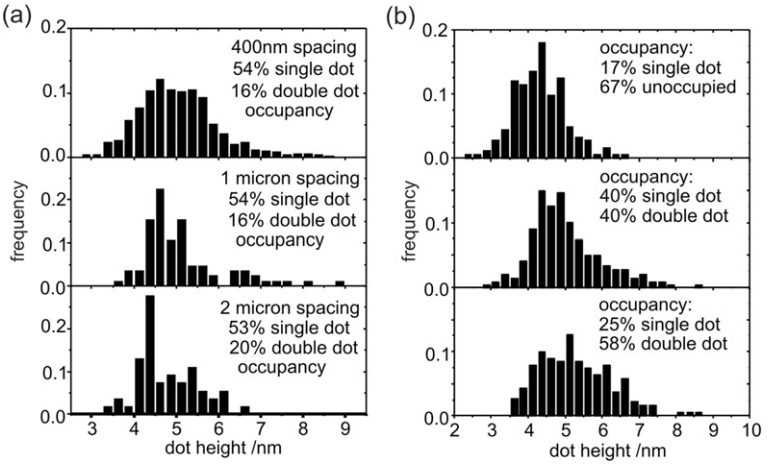

Fig. 7. Dot height histograms for single occupied sites: (a) with different site spacings (b) with different pattern sizes and deposition amounts. Data taken over a 100 μm^2 area to get reasonable statistics [60]. Part reprinted from [60] with permission from Elsevier.

used for the modeled curve and the scatter in the data due to error in the AFM measurement of both the hole size and dot volume. There is some discrepancy between the model and the experimental data, most noticeable in the 1.9 ML ($0.8C_{\text{crit}}$) data at the onset of dot formation which is likely to be due to the use of a power-law fit in Fig. 6(c) which exaggerates the initial increase in dot volume [59] and in the 2.1 ML ($0.95C_{\text{crit}}$) data at the larger pattern sizes which is probably due to the onset of dot coalescence leading to incoherent dots at multiply occupied sites which then act as efficient capture sites for indium adatoms [12]. This discrepancy may also be a sign of some contribution of strain-driven net migration towards the pattern sites. However, given the good fit of the 2.0 ML ($0.85C_{\text{crit}}$) data, this contribution, if present, is likely to be small. Therefore, it seems adequate to consider growth of the site-controlled dots as being determined by a localized modification of the surface strain over an infilled hole.

4. Size control of site-controlled dots

To achieve good coupling between the emission from a quantum dot and from a photonic cavity it is not sufficient to control the position of the quantum dot, it is also necessary to control the dot size so that the emission wavelength of the dot is close enough to that of the cavity [5] in order to bring the two into resonance (see for example Ref. [7]). Ultimately the aim will be to have site-controlled dots emitting at one of the telecommunication wavelengths, such as 1.3 μm [18,23].

4.1. Effect of pattern spacing

When considering overgrowth of these dilute arrays, it is important to consider whether the pattern spacing has any effect. Fig. 7(a) shows the average occupancy and the size distribution of site controlled dots on singly-occupied sites for 400 nm, 1 μm and 2 μm pattern spacings [60]. Data are not shown for spacings smaller than 400 nm as for denser arrays because the patterns became irregular during the 10 nm GaAs buffer growth, affecting the dot formation.

No significant change in either the occupancy or dot size can be seen in Fig. 7(a), implying that the effect of the pattern spacing is very small. This supports the conclusion in the previous section that the mechanism for these site-controlled dots is mainly a localized modification of the surface strain. This is different to the growth of stacked, dense ordered arrays (spacing $\sim$200 nm) where the occupancy is sensitive to changes in pattern spacing of $\sim$50 nm [37].

4.2. Effect of pattern size and deposition amount

In Fig. 5(c) we showed that the pattern occupancy can be increased either by increasing the pattern size or the InAs deposition amount, and that a change in pattern size can be related to a change in the local critical thickness. Therefore we can use the pattern occupancy as a measure of the deposition amount above the critical thickness on a patterned

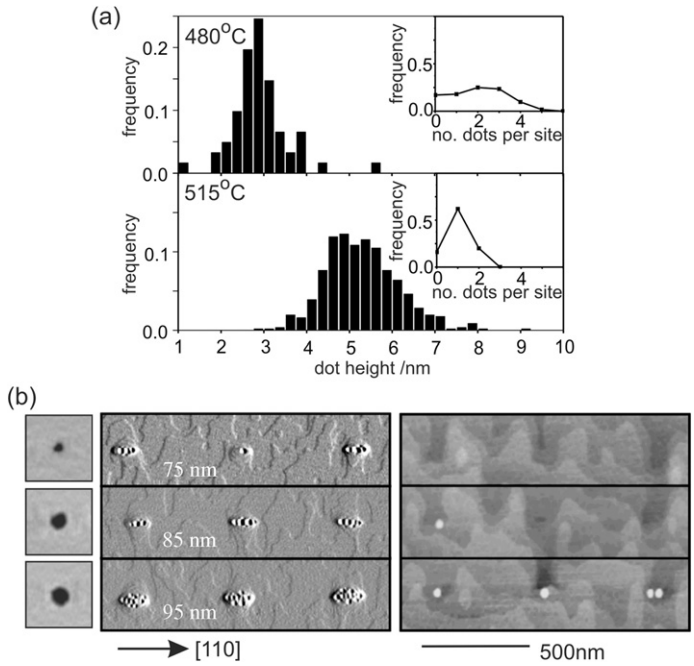

Fig. 8. (a) Dot height histograms for singly occupied sites at a growth temperature of 480 °C (top panel) and 515 °C (bottom panel). The insets show the dot occupancy distribution at these temperatures for patterns ∼95 nm wide and ∼13 nm (∼15 nm) deep for the 480 °C (515 °C) data respectively following $\sim 0.9C_{\text{crit}}$ InAs deposition. (b) AFM images of the patterned hole and the dot occupancy following overgrowth of a 10 nm GaAs buffer and $\sim 0.9C_{\text{crit}}$ InAs deposition at 480 °C (left) and 515 °C (right). The 480 °C AFM image shows variation in cantilever amplitude, which is proportional to surface gradient, for improved contrast. The pattern sizes were ∼13 nm deep and ∼75 nm wide (top), ∼85 nm wide (middle) and ∼95 nm wide (bottom).

site, irrespective of whether the occupancy was controlled by changing the deposition amount or the pattern size. This is supported by the observation that there is no difference in the dot size distribution on patterns which have a similar occupancy even if different amounts of InAs were deposited [60].

Fig. 7(b) shows the change in the dot height distribution for dots on singly occupied sites with increasing pattern occupancy [60]. The dot height slowly increases as the occupancy increases. This is similar to the behaviour on a planar surface shown in Fig. 1(c) where a rapid increase in density is seen together with a slow increase in dot size with increasing deposition amount. This means that it is not possible to tune the site-controlled dot height independently of the site occupancy simply by controlling the deposition amount or the pattern size.

4.3. Effect of growth temperature and growth rate

Fig. 8(a) demonstrates the effect of the substrate temperature on the size of the site-controlled dots, showing that reducing the substrate temperature also reduces the size of the dots – in exactly the same manner as growth of dots on unpatterned substrates. The insets to Fig. 8(a) shows that relatively good, i.e. >20% single-dot occupancy can be achieved even at low dot growth temperatures, showing that a long InAs migration length is not necessary to achieve selective dot nucleation on a dilute ordered array [61].

However, from the inserts to Fig. 8(a) it can be seen that the spread of the occupancy distribution is broader at lower temperatures. This means that the occupancy is much more sensitive to fluctuations in the initial pattern size at the lower temperatures. Compared to high dot growth temperatures (∼510 °C) where changes in the pattern size of ∼10 nm lead to a change in occupancy by one dot (see Fig. 5(a)), at the lower temperatures (∼480 °C) this small fluctuation in pattern size can lead to a change in occupancy of two dots. This sensitivity to pattern size fluctuation is also related to the optimal pattern size for site-control. Fig. 8(b) demonstrates that the optimal pattern size for single dot site control is dependent on the growth temperature. A pattern size which gives good single dot site control at

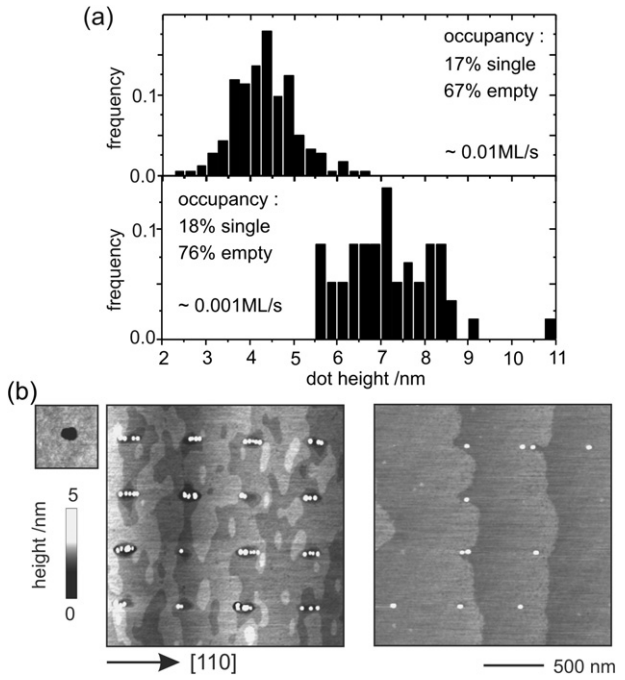

Fig. 9. (a) Dot height histograms for singly occupied sites at a growth rate of 0.01 ML/s (top panel) and 0.001 ML/s (bottom panel) for similar pattern occupancies. The pattern size was ∼20 nm deep and ∼80 nm (∼150 nm) wide for the 0.01 ML/s (0.001 ML/s) sample. (b) (left to right) AFM images of the patterned hole, the dot occupancy following overgrowth of a 10 nm GaAs buffer and $0.88C_{\text{crit}}$ InAs at 0.01 ML/s (left image), and after $0.96C_{\text{crit}}$ InAs at 0.001 ML/s (right image). The pattern size is ∼150 nm wide and ∼20 nm deep.

∼510 °C is clearly too large for single dot site control at 480 °C. Therefore smaller pattern sizes are required to give good single dot site control at lower dot growth temperatures.

The relationship between the optimal pattern size for single dot site-control and the dot growth temperature can be understood by considering the effect of the substrate temperature on dot growth on a planar region. Reduction of the growth temperature leads to a much more rapid increase in dot density with deposition amount, and an overall higher dot density. When considering the dot growth over the patterned hole site, this should proceed in the same manner as growth on a planar region, the main effect of the patterning being that dot nucleation occurs sooner over the patterned site due to the presence of some in-built strain in the surface. Therefore, the fact that a reduction in growth temperature leads to a much higher dot density translates directly to a much higher dot occupancy over a given patterned hole area, and a much more rapid change in occupancy with change in pattern size, as has been observed.

Fig. 9(a) shows that the dot height can be increased, in the same way as on a planar substrate, by decreasing the growth rate, from 0.01 ML/s to 0.001 ML/s and a similar degree of site selectivity can be achieved. However, as discussed above, the optimal pattern size depends on the growth conditions. Fig. 9(b) shows that a patterned hole ∼150 nm wide, ∼20 nm deep is far too large, leading to ∼4 dots nucleating per patterned site after $0.88C_{\text{crit}}$ is deposited at 0.01 ML/s. However, the same patterned site leads to ∼1 dot nucleating per patterned site after $0.96C_{\text{crit}}$ is deposited at 0.001 ML/s. Therefore the optimal pattern size for site-control of single dots increases as the growth rate decreases. This is related to the decrease in dot density as the growth rate decreases, meaning that a larger area with a locally reduced critical thickness is required to have a high probability of a dot nucleating there.

5. Photoluminescence of site-controlled dots

To incorporate a dot deterministically into a photonic cavity for quantum information applications, not only does the dot position and size need to be controllable, but luminescence from these dots must also be observable. Ideally this luminescence should be bright i.e. there should be very few other possible recombination paths in the surroundings of the dot, so that emitted single photons can be detected. Also many quantum information proposals require two indistinguishable photons [62] for which the dot radiative lifetime needs to be much shorter than the decoherence

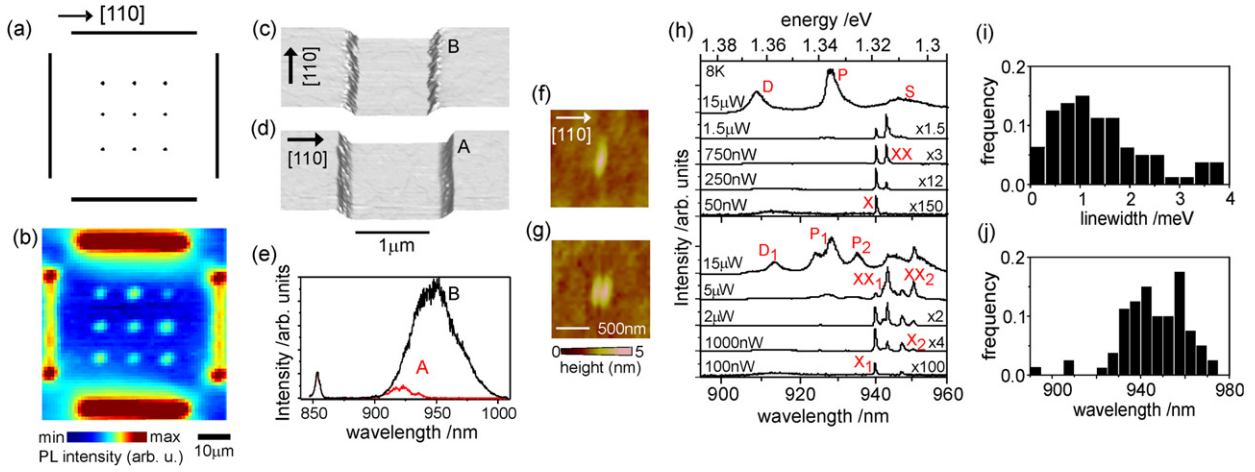

Fig. 10. (a) Schematic of the initial etched pattern consisting of a 3 × 3 array of small holes spaced 10 microns apart surrounded by 1 micron wide trenches etched for alignment purposes. (b) Integrated PL intensity map (integration range 900–1000 nm) of capped InAs dots grown over the etched pattern. Dot luminescence can be seen from all the etched areas [44]. (c) and (d) 3D AFM images of the nominally 1 micron wide trenches after overgrowth with an 8nm GaAs buffer and 1.4 ML InAs along the [110] direction with B-type step edges, and along the [−110] direction with A-type step edges respectively. (e) PL spectrum from the two different types of trenches showing much greater luminescence from trenches aligned along the [110] direction due to the greater dot density on the B-type step edges. (f) and (g) AFM height images of the GaAs surface above a patterned site where 2 nm high mounds indicate the occupancy of the site showing (f) one site-controlled dot and (g) pair of site-controlled dots. (h) Power dependence of the luminescence from a single site-controlled dot (top panel) and a pair of dots (lower panel). Emission from the exciton is labeled as X, biexciton as XX, excited states as P and D. (i) Histogram of the linewidth of the quantum dot emission at low power (< 1 μW) from 80 site-controlled dots. (j) Histogram of the ground state emission from 80 site-controlled dots.

time [63]. Both these properties, luminescence efficiency and radiative lifetime, can, to some extent, be improved by the device structure containing the dot [1,63]; however ultimately, the properties of a site-controlled dot should be as good as that of randomly grown quantum dots.

To study the luminescence properties the dots were capped with GaAs consisting of a 1.5 nm GaAs cap at the same substrate temperature as the dot growth, followed by a 2 min anneal under As_4 at 570 °C. This partial cap and anneal limits the dot emission wavelength to ∼940 nm. The growth was then finished with a final 70 nm GaAs cap at 570 °C. Even after this final cap layer, the surface morphology still showed a mound ∼2 nm high over an underlying dot, allowing the number of site-controlled dots at a patterned site to be determined by AFM as can be seen in Figs. 10(f) and 10(g).

Micro-photoluminescence (PL) measurements were carried out at 8 K using a 532 nm cw frequency doubled Nd:YVO_4 laser. The laser was focused to a spot of ∼1.5 μm diameter and the sample was moved using motorized x–y stages allowing us to map the PL emission. The PL signal was dispersed by a spectrometer with 500 mm focal length and detected with a liquid nitrogen cooled Si-CCD detector.

Fig. 10(a) shows a schematic of the pattern used for PL investigation. The pattern consists of a 3 × 3 array of small holes spaced 10 μm apart surrounded by alignment markers consisting of 1 μm wide trenches which are visible under an optical microscope. Fig. 10(b) shows a spatial map of the integrated PL intensity, (integration range 900–1000 nm) for this pattern. Emission from QDs is only seen from the etched areas, with emission from both the patterned hole sites and the alignment trenches. There is a high dot density at the step edges of the etched trenches as shown in the AFM image of an uncapped sample in Figs. 10(c) and 10(d). A higher dot density can be seen along the B-type step edges, which leads to brighter emission from the trenches parallel to [110] as is clearly seen by the luminescence spectrum in Fig. 10(e)). Fig. 10(e) also shows that slightly longer wavelength emission is observed on the B-type trenches, implying that not only is the dot density higher here, but that the dots are also larger due to the greater probability of adatom capture on these steps.

Fig. 10(h) shows PL from two different pattern sites, one containing a single site-controlled dot and one containing a pair of site-controlled dots, as can be seen from the surface morphology shown in Figs. 10(f) and 10(g) respectively [44]. For the single dot in Fig. 10(h) a single line, 500 μeV wide, is seen at low power, attributed to the neutral exciton emission. A second line is apparent by 100 nW incident power and dominant by 750 nW, which we attribute

to the biexciton. Its binding energy is 3.9 meV, which is typical for dots emitting at this wavelength [64]. At powers greater than 2 μW the excited states can also be seen, with 23 meV and 28 meV separation for the S-P and P-D shells respectively. This is lower than typically seen for dots emitting at this wavelength [65] indicating that there is strong intermixing of the In(Ga)As, driven by the hole curvature as the hole becomes infilled. This would lead to an InGaAs layer below the site-controlled dot, lowering the confinement energy. This is supported by the observation that in general the site-controlled dots are slightly shorter than those grown at the same temperature on a planar substrate [60]. For the pair of site-controlled dots emission from each dot, separated in energy by 10 meV, can be seen, and the power dependence, linewidth and energy spacing of each dot is similar to that of the single dot. More detailed discussion of the power dependence is given elsewhere [44].

The emission from these dots is typical in behaviour of randomly grown, defect free dots. However, the luminescence is clearly affected by the presence of the regrowth interface, which is within 8 nm from these dots. This is evidenced by the fact that, similar to other studies of single site-controlled dots [39,40,34], the peak luminescence from these dots is a factor of ten times weaker compared to that from dots situated far from any interfaces, and the linewidths at low excitation power are broad, ranging from 200 μeV to > 3 meV, for 80 site-controlled dots measured, as shown in Fig. 10(j). This indicates both the presence of non-radiative defects at the regrowth interface and a fluctuating charge background caused by carrier trapping at these defects. These defects are likely to be deep level electron traps such as the Ga_{As} defect [66] since the surface is generally left disordered [51] and slightly arsenic deficient following deoxidation [46,47] with a defect density of $\sim 3 \times 10^{11}$ cm^{-2} [67].

It is possible that this defect density could be reduced both by controlling the surface contamination and oxide stoichiometry carefully after patterning, for example by the use of UV ozone grown oxides to create a more arsenic rich oxide surface [68] to reduce the surface disorder following deoxidation, or by avoiding the growth of a native oxide altogether by keeping the patterned substrate under a nitrogen environment after the final oxide removal stage [69]. However the easiest way to improve the luminescence properties may be to simply increase the separation of the dots from the buried interface to ~ 40 nm in the same way as luminescence from near-surface dots is not degraded by the surface once the dots are separated by ~ 40 nm from the air-interface [70].

Increasing the dot-regrowth interface separation to ~ 40 nm cannot be achieved by a single layer due to the change in hole shape which occurs during the buffer growth thus limiting the buffer thickness. However, it can be achieved by the growth of vertically stacked layers where the strain field above a buried dot determines the position of a dot in the second layer, for spacer thicknesses of up to ~ 20 nm between the two layers [71,72]. The emission wavelength of the dots in each layer can be tuned independently by suitable choice of growth conditions (see for example Ref. [73]). Such a technique has been successfully demonstrated on dense ordered arrays (spacing ~ 200 nm), with as good luminescence from a patterned area as from an unpatterned area being observed after several stacked layers were grown [74].

Finally, it is worth noting that the range of wavelengths of these widely spaced site-controlled dots, shown in Fig. 10(j) corresponds to a 40 meV inhomogeneous broadening, which is comparable to that seen on an unpatterned surface under similar growth conditions. This effectively illustrates that these sites are uncorrelated and that each patterned site only locally modifies the surface strain to lead to preferential dot formation, such that fluctuations in the pattern size lead to fluctuations in the eventual dot size.

6. Conclusion and future outlook

We have demonstrated here the use of ex-situ electron beam patterned substrates to control the nucleation site of InAs quantum dots. This site-control has been shown to be due to the difference in strain above the patterned site after it has infilled compared to the surrounding planar area. We have shown that the occupancy of these patterned sites can be controlled both by the pattern size and the InAs deposition amount, and that the size of these dots can be controlled by varying the growth conditions in the same way as conventional, randomly distributed quantum dots, while still maintaining good site-control.

However, although these site-controlled dots are coherent and demonstrate similar luminescence in terms of energy levels and power dependence as conventionally grown dots, the luminescence properties such as emission intensity and linewidth are strongly dependent on the local environment and so are clearly affected by the vicinity of the regrowth interface. Since *ex-situ* patterning has a distinct advantage over any *in-situ* patterning technique due to its flexibility and ease of subsequent integration with further device processing post-growth, the remaining challenge is

to minimize the effect of this interface on the luminescence properties. One way to do this may be to simply grow vertically stacked layers of dots above a site-controlled dot, with the top dot spectrally isolated from the lower ones.

Acknowledgements

This work was financially supported by the BMBF (01BM459), the DFG research group "Positioning of single nanostructures – singe quantum devices" (FOR 730), and the EPSRC and DTI via the Optical Systems for the Digital Age "QLED" project.

References

[1] J.M. Gerard, Topics Appl. Phys. 90 (2003) 269.
[2] B. Lounis, M. Orrit, Rep. Prog. Phys. 68 (2005) 1129.
[3] A.J. Shields, Nat. Photon. 1 (2007) 215.
[4] O.G. Schmidt (Ed.), Lateral Alignment of Epitaxial Quantum Dots, Springer, Berlin, 2007.
[5] E.M. Purcell, Phys. Rev. 69 (1946) 681.
[6] K.H. Lee, A.M. Green, R.A. Taylor, D.N. Sharp, J. Scrimgeour, O.M. Roche, J.H. Na, A.F. Jarjour, A.J. Turberfield, F.S.F. Brossard, D.A. Williams, G.A.D. Briggs, Appl. Phys. Lett. 88 (2006) 193106.
[7] K. Hennessy, A. Badolato, M. Winger, D. Gerace, M. Atatüre, S. Gulde, S. Fält, E.L. Hu, A. Imamoğlu, Nature 445 (2007) 896.
[8] B.A. Joyce, D.D. Vvedensky, Mater. Sci. Eng. Reports 46 (2004) 127.
[9] E. Placidi, F. Arciprete, M. Fanfoni, F. Patella, A. Balzarotti, in: Z.M. Wang (Ed.), Self-assembled Quantum Dots, in: Lecture Notes in Nanoscale Science and Technology, Springer, New York, 2008, p. 1.
[10] D. Bimberg, M. Grundmann, N.N. Ledentsov, Quantum dot Heterostructures, John Wiley and Sons Ltd, Chichester, 1999.
[11] F. Patella, F. Arciprete, M. Fanfoni, A. Balzarotti, E. Placidi, Appl. Phys. Lett. 88 (2006) 161903.
[12] D. Leonard, K. Pond, P.M. Petroff, Phys. Rev. B 50 (1994) 11687.
[13] R. Leon, T.J. Senden, Y. Kim, C. Jagadish, A. Clark, Phys. Rev. Lett. 78 (1997) 4942.
[14] E. Placidi, F. Arciprete, V. Sessi, M. Fanfoni, F. Patella, A. Balzarotti, Appl. Phys. Lett. 86 (2005) 241913.
[15] D. Bimberg, M. Grundmann, N.N. Ledentsov, S.S. Ruvimov, P. Werner, U. Richter, J. Heydenreich, V.M. Ustinov, P.S. Kop'ev, Zh.I. Alferov, Thin Solid Films 267 (1995) 32.
[16] G.S. Solomon, S. Komarov, J.S. Harris Jr., J. Cryst. Growth 201–202 (1999) 1190.
[17] P.M. Lytvyn, V.V. Strelchuk, O.F. Kolomys, I.V. Prokopenko, M.Ya. Valakh, Yu.I. Mazur, Zh.M. Wang, G.J. Salamo, M. Hanke, Appl. Phys. Lett. 91 (2007) 173118.
[18] B. Alloing, C. Zinoni, V. Zwiller, L.H. Li, C. Monat, M. Gobet, G. Buchs, A. Fiore, E. Pelucchi, E. Kapon, Appl. Phys. Lett. 86 (2005) 101908.
[19] Y. Nakata, K. Mukai, M. Sugawara, K. Ohtsubo, H. Ishikawa, N. Yokoyama, J. Cryst. Growth 208 (2000) 93.
[20] G. Costantini, A. Rastelli, C. Manzano, P. Acosta-Diaz, G. Katsaros, R. Songmuang, O.G. Schmidt, H.v. Känel, K. Kern, J. Cryst. Growth 278 (2005) 38.
[21] M.C. Xu, Y. Temko, T. Suzuki, K. Jacobi, J. Appl. Phys. 98 (2005) 083525.
[22] S. Kiravittaya, A. Rastelli, O.G. Schmidt, Appl. Phys. Lett. 87 (2005) 243112.
[23] M.B. Ward, O.Z. Karimov, D.C. Unitt, Z.L. Yuan, P. See, D.G. Gevaux, A.J. Shields, P. Atkinson, D.A. Ritchie, Appl. Phys. Lett. 86 (2005) 201111.
[24] S. Anders, C.S. Kim, B. Klein, M.W. Keller, R.P. Mirin, A.G. Norman, Phys. Rev. B 66 (2002) 125309.
[25] I. Mukhametzhanov, Z. Wei, R. Heitz, A. Madhukar, Appl. Phys. Lett. 75 (1999) 85.
[26] G.S. Solomon, J.A. Trezza, J.S. Harris Jr., Appl. Phys. Lett. 66 (1995) 991.
[27] M. Kitamura, M. Nishioka, J. Oshinowo, Y. Arakawa, Appl. Phys. Lett. 66 (1995) 3663.
[28] H. Lee, J.A. Johnson, J.S. Speck, P.M. Petroff, J. Vac. Sci. Technol. B 18 (2000) 2193.
[29] T.v. Lippen, R. Nötzel, G.J. Hamhuis, J.H. Wolter, Appl. Phys. Lett. 85 (2004) 114.
[30] D.S.L. Mui, D. Leonard, L.A. Coldren, P.M. Petroff, Appl. Phys. Lett. 66 (1995) 1620.
[31] R. Zhang, R. Tsui, K. Shiralagi, D. Convey, H. Goronkin, Appl. Phys. Lett. 73 (1998) 505.
[32] M. Mehta, D. Reuter, A. Melnikov, A.D. Wieck, A. Remhof, Appl. Phys. Lett. 91 (2007) 123108.
[33] S. Kohmoto, H. Nakamura, T. Ishikawa, S. Nishikawa, T. Nishimura, K. Asakawa, Mater. Sci. Eng. B 88 (2002) 292.
[34] H.Z. Song, T. Usuki, T. Ohshima, Y. Sakuma, M. Kawabe, Y. Okada, K. Takemoto, T. Miyazawa, S. Hirose, Y. Nakata, M. Takatsu, N. Yokoyama, Nanoscale Res. Lett. 1 (2006) 160.
[35] S. Jeppesen, M.S. Miller, B. Kowalski, I. Maximov, L. Samuelson, Superlatt. Microstruct. 23 (1998) 1347.
[36] Y. Nakamura, N. Ikeda, S. Ohkouchi, Y. Sugimoto, H. Nakamura, K. Asakawa, Physica E 21 (2004) 551.
[37] S. Kiravittaya, H. Heidemeyer, O.G. Schmidt, Physica E 23 (2004) 253.
[38] H. Heidemeyer, C. Müller, O.G. Schmidt, J. Cryst. Growth 261 (2004) 444.
[39] P. Atkinson, M.B. Ward, S.P. Bremner, D. Anderson, T. Farrow, G.A.C. Jones, A.J. Shields, D.A. Ritchie, Jpn. J. Appl. Phys. 45 (2006) 2519.
[40] T. Sünner, C. Schneider, M. Strauß, A. Huggenberger, D. Wiener, S. Höfling, M. Kamp, A. Forchel, Opt. Lett. 33 (2008) 1759.
[41] S. Osakabe, S. Adachi, Jpn. J. Appl. Phys. 36 (1997) 7119.

[42] Z.R. Wasilewski, J.-M. Baribeau, M. Beaulieu, X. Wu, G.I. Sproule, J. Vac. Sci. Technol. B 22 (2004) 1534.
[43] P. Atkinson, O.G. Schmidt, J. Cryst. Growth, in press, doi: 10.1016/j.jcrysgro.2008.09.024.
[44] P. Atkinson, S. Kiravittaya, M. Benyoucef, A. Rastelli, O.G. Schmidt, Appl. Phys. Lett. 93 (2008) 101908.
[45] F. Proix, C.A. Sébenne, M. Cherchour, O. M'hamedi, J.P. Lacharme, J. Appl. Phys. 64 (1998) 898.
[46] E.J. Petit, F. Houzay, J. Vac. Sci. Technol. B 12 (1884) 547.
[47] P. Tomkiewicz, A. Winkler, J. Szuber, Appl. Surf. Sci. 252 (2006) 7647.
[48] J.H. Lee, Zh.M. Wang, G.J. Salamo, J. Appl. Phys. 100 (2006) 114330.
[49] P. Atkinson, S.P. Bremner, D. Anderson, G.A.C. Jones, D.A. Ritchie, Microel. J. 37 (2006) 1436.
[50] S.I. Yi, P. Kruse, M. Hale, A.C. Kummel, J. Chem. Phys. 114 (2001) 3215.
[51] A. Khatiri, J.M. Ripalda, T.J. Krzyzewski, G.R. Bell, C.F. McConville, T.S. Jones, Surf. Sci. 548 (2004) L1.
[52] X.-Q. Shen, D. Kishimoto, T. Nishinaga, Jpn. J. Appl. Phys. 33 (1994) 11.
[53] K. Shiraishi, Y.Y. Suzuki, H. Kageshima, T. Ito, Appl. Surf. Sci. 130–132 (1998) 431.
[54] E.S. Tok, J.H. Neave, J. Zhang, B.A. Joyce, T.S. Jones, Surf. Sci. 374 (1997) 397.
[55] T. Ogura, T. Nishinaga, J. Cryst. Growth 211 (2000) 416.
[56] M. Ozdemir, A. Zangwill, J. Vac. Sci. Technol. A 10 (1992) 684.
[57] E. Kapon, E. Pelucchi, S. Watanabe, A. Malko, M.H. Baier, K. Leifer, B. Dwir, F. Michelini, M.-A. Dupertuis, Physica E 25 (2004) 288.
[58] L. Wang, A. Rastelli, S. Kiravittaya, P. Atkinson, F. Ding, C.C. Bof Bufon, C. Hermannstädter, M. Witzany, G.J. Beirne, P. Michler, O.G. Schmidt, New J. Phys. 10 (2008) 045010.
[59] H.T. Dobbs, D.D. Vvedensky, A. Zangwill, Appl. Surf. Sci. 123 (1998) 646.
[60] P. Atkinson, M.B. Ward, S.P. Bremner, D. Anderson, T. Farrow, G.A.C. Jones, A.J. Shields, D.A. Ritchie, Physica E 32 (2006) 21.
[61] P. Atkinson, S.P. Bremner, D. Anderson, G.A.C. Jones, D.A. Ritchie, J. Vac. Sci. Technol. B 24 (2006) 1523.
[62] E. Knill, R. Laflamme, G.J. Milburn, Nature 409 (2001) 46.
[63] C. Santori, D. Fattal, J. Vučković, G.S. Solomon, Y. Yamamoto, Nature 419 (2002) 594.
[64] S. Rodt, A. Schliwa, K. Pötschke, F. Guffarth, D. Bimberg, Phys. Rev. B 71 (2005) 155325.
[65] S. Fafard, C.Nì. Allen, Appl. Phys. Lett. 75 (1999) 2374.
[66] W.E. Spicer, Z. Liliental-Weber, E. Weber, N. Newman, T. Kendelewicz, R. Cao, C. McCants, P. Mahowald, K. Miyano, I. Lindau, J. Vac. Sci. Technol. B 6 (1988) 1245.
[67] T.M. Burke, E.H. Linfield, D.A. Ritchie, M. Pepper, J.H. Burroughes, J. Cryst. Growth 175 (1997) 416.
[68] M.G. Proietti, J. Garcia, J. Chaboy, F. Morier-Genoud, D. Martin, J. Phys. Condens. Matter 5 (1993) 1229.
[69] O.E. Tereshchenko, S.I. Chikichev, A.S. Terekhov, J. Vac. Sci. Technol. A 17 (1999) 2655.
[70] C.F. Wang, A. Badolato, I. Wilson-Rae, P.M. Petroff, E. Hu, J. Urayama, A. Imamoğlu, Appl. Phys. Lett. 85 (2004) 3423.
[71] Q. Xie, J.L. Brown, R.L. Jones, J.E. Van Nostrand, K.D. Leedy, Appl. Phys. Lett. 76 (2000) 3082.
[72] M.O. Lipinski, H. Schuler, O.G. Schmidt, K. Eberl, N.Y. Jin-Phillipp, Appl. Phys. Lett. 77 (2000) 1789.
[73] I. Mukhametzhanov, R. Heitz, J. Zeng, P. Chen, A. Madhukar, Appl. Phys. Lett. 73 (1998) 1841.
[74] S. Kiravittaya, A. Rastelli, O.G. Schmidt, Appl. Phys. Lett. 88 (2006) 043112.